Analog beamforming for Full-Duplex millimeter wave communication

Roberto López-Valcarce
atlanTTic Research Center – University of Vigo, Spain
valcarce@gts.uvigo.es

Nuria González-Prelcic
University of Texas at Austin
ngprelcic@utexas.edu

***Abstract*—Full-duplex (FD) communication has the potential for significant improvements in spectral efficiency, as long as the problem of self-interference (SI) can be overcome. For millimeter wave (mmWave) systems with large antenna arrays, beamforming based SI mitigation is attractive because of the large number of degrees of freedom available. Previously proposed precoder-combiner designs, however, suffer from a large performance loss under the hardware-constrained architectures required for operation at mmWave. In this context, we develop a new algorithm for the design of constant-amplitude analog precoders and combiners of an FD mmWave single-stream bidirectional link, significantly reducing the aforementioned performance loss.**

***Index Terms*—Full-duplex, millimeter wave communications, analog beamforming.**

I. Introduction

Multiple-input multiple-output (MIMO) systems operating at millimeter wave (mmWave) frequencies enable applications needing several Gbits/s data rates [1]. Some mmWave products compliant with the IEEE 802.11ad standard are already in the market. The first release of the 5G standard for cellular networks has been recently approved [2], defining a system capable to operate at sub-6 GHz as well as mmWave frequencies. Several challenges to practical mmWave communications, such as analog beamforming or the design of hybrid precoders [1], have been extensively studied in the last few years, but many questions remain open. For example, preliminary studies have considered the feasibility of transmitting on one mmWave base station panel while simultaneously receiving on an adjacent panel [3], [4]. In general, the design of such full-duplex (FD) mmWave systems is an open problem.

FD wireless communication, by which a transceiver simultaneously transmits and receives on the same frequency channel, has recently attracted the attention of researchers due to its potential to double spectral efficiency with respect to traditional half-duplex schemes [5], [6]. However, it brings about the problem of *self-interference* (SI): an FD node's own transmission will be present at its receive side, typically with a power level tens of dB above that of the signal of interest from a remote node. Managing SI constitutes the main challenge for the development of FD wireless communication.

Work supported in part by the Agencia Estatal de Investigación (Spain), in part by the European Regional Development Fund (ERDF) through projects WINTER (TEC2016-76409-C2-2-R) and MYRADA (TEC2016-75103-C2-2-R), and in part by the Xunta de Galicia (Agrupación Estratéxica Consolidada de Galicia accreditation 2016-2019).

Significant SI mitigation has been demonstrated for a microwave-band, single-antenna FD node [7], [8] by combining *propagation domain* methods (radiation pattern optimization, antenna placement, etc.), *analog-circuit domain* methods (which substract an SI estimate from the received signal before the A/D converter to avoid its saturation), and *digital domain* methods (which attempt to estimate and substract any residual SI after A/D conversion). Direct extension to MIMO FD is difficult, because analog-circuit domain methods do not scale well with the number of antennas. *Spatial suppression,* i.e., exploiting the availability of multiple antennas to mitigate SI in MIMO FD by means of digital precoding and combining, has been proposed as an alternative [11]–[13], although such approach results in lower data rates since some of the available spatial degrees of freedom (DoF) are spent in mitigating SI.

In contrast with microwave-band systems, large antenna arrays are generally required in mmWave communication. The available DoF are substantially larger, making spatial suppression attractive for FD operation. For example, in [15] a method with close to optimal performance was proposed for the design of the (digital baseband) beamforming weights of an FD mmWave single-stream bi-directional link. On the other hand, to reduce power consumption and cost, hybrid architectures [1], [14] are preferred in mmWave, by which a reduced number of RF chains is used and the transmit/receive processing is partitioned between the digital baseband and analog RF domains. Analog precoders/combiners are then implemented with low-cost phase shifters, resulting in additional design constraints, i.e., it is not possible to alter the magnitude of the RF signals. Spatial suppression methods for SI management in FD mmWave systems must take such hardware-related, constant-amplitude (CA) constraints into account. In particular, as shown in [16], it is not straightforward to incorporate CA constraints into the quasi-optimal design from [15]: for instance, merely projecting the optimal unconstrained weights onto the manifold defined by the CA constraints incurs a large performance loss, as recognized in [16]. Another approach suggested in [16] is to constrain each beamforming weight vector to the manifold of steering vectors (which comply to the CA constraints), parameterized by a single steering angle; a search over the (four-dimensional) steering angle space then provides the sought beamformers. However, this search may be prohibitively complex if fine angle resolution is desired, and even then the final performance is largely

degraded [16]. Finally, although it is possible to circumvent the CA constraints by doubling the number of transmit and receive RF chains [9], [16], or by using two phase shifters for each coefficient [10], those approaches increase transceiver cost and power consumption.

We present a novel design to explicitly account for CA constraints, overcoming the limitations of the different approaches in [16]. The proposed method significantly reduces the aforementioned loss, performing almost as well as the all-digital design. In this way, suitable analog beamformers for FD mmWave operation are obtained at reasonable computational cost, cancelling SI in the analog domain, and without the need to double the number of RF chains or phase shifters.

II. Problem setting

Fig. 1 represents a mmWave network of two nodes in FD mode. Each node is equipped with transmit (TX) and receive (RX) antenna arrays, with a single data stream supported in each direction. The number of transmit antennas at node i and of receive antennas at node j are respectively denoted as $N_{t,i}$ and $N_{r,j}$, with $i, j \in \{1, 2\}$. The transmission bandwidth is assumed sufficiently narrow so that channels can be regarded as frequency-flat. We denote $\boldsymbol{H}_{ij}$ the $N_{r,j} \times N_{t,i}$ channel matrix from the TX array of node i to the RX array of node j. Note that $\boldsymbol{H}_{jj}$ corresponds to the SI channel affecting node j. We postpone a discussion on specific channel models to the description of simulation results in Sec. V, since the designs to be presented next are model-independent.

Let $\boldsymbol{f}_i$ denote the complex-valued $N_{t,i} \times 1$ beamforming vector (precoder) applied by node $i \in \{1, 2\}$ before transmission; and let $\boldsymbol{w}_j$ denote the $N_{r,j} \times 1$ combiner applied by node $j \in \{1, 2\}$ after reception. With analog-domain beamforming using phase shifters, each of the entries of these vectors has constant magnitude, and it is only possible to pick their phases. The average transmit power per symbol of node i is ρ_i, and the noise $\boldsymbol{n}_j$ at the receiver of node j is zero-mean white Gaussian with covariance $\sigma_j^2 \boldsymbol{I}_{N_{r,j}}$. With these, the received symbols at nodes 1 and 2 are respectively given by

$$y_1 = \boldsymbol{w}_1^H \left(\sqrt{\rho_2}\boldsymbol{H}_{21}\boldsymbol{f}_2 s_2 + \sqrt{\eta_1}\boldsymbol{H}_{11}\boldsymbol{f}_1 z_1 + \boldsymbol{n}_1\right), \quad (1)$$

$$y_2 = \boldsymbol{w}_2^H \left(\sqrt{\rho_1}\boldsymbol{H}_{12}\boldsymbol{f}_1 s_1 + \sqrt{\eta_2}\boldsymbol{H}_{22}\boldsymbol{f}_2 z_2 + \boldsymbol{n}_2\right), \quad (2)$$

with s_i the zero-mean unit-variance symbol sent by node i. The zero-mean unit-variance SI affecting node j is denoted by z_j, and η_j quantifies SI strength. Due to front-end imperfections, in general z_j will be a distorted version of the signal transmitted by node j [11]; if any propagation and/or analog-circuit domain SI mitigation method is applied, then z_j is to be understood as the residual SI. To meet the TX power constraint, $\|\boldsymbol{f}_i\| = 1$ is imposed, $i \in \{1, 2\}$.

Treating SI as noise and assuming Gaussian codebooks, the sum rate of this network can be written as

$$\mathcal{R} = \log_2\left(1 + \frac{\rho_2|\boldsymbol{w}_1^H\boldsymbol{H}_{21}\boldsymbol{f}_2|^2}{\sigma_1^2\boldsymbol{w}_1^H\boldsymbol{w}_1 + \eta_1|\boldsymbol{w}_1^H\boldsymbol{H}_{11}\boldsymbol{f}_1|^2}\right) + \log_2\left(1 + \frac{\rho_1|\boldsymbol{w}_2^H\boldsymbol{H}_{12}\boldsymbol{f}_1|^2}{\sigma_2^2\boldsymbol{w}_2^H\boldsymbol{w}_2 + \eta_2|\boldsymbol{w}_2^H\boldsymbol{H}_{22}\boldsymbol{f}_2|^2}\right). \quad (3)$$

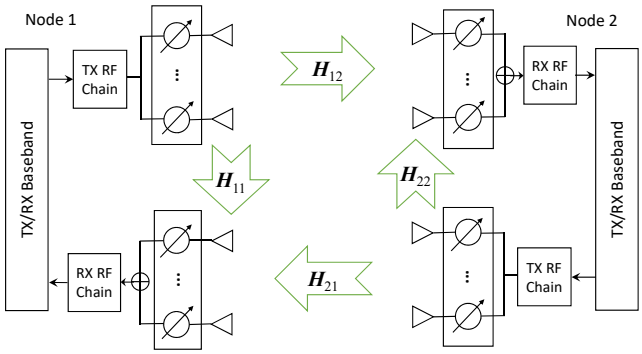

Fig. 1. Two-node FD network with analog TX/RX beamforming.

$\mathcal{R}$ is invariant to scalings of $\boldsymbol{w}_j$, so $\|\boldsymbol{w}_j\| = 1$, $j \in \{1, 2\}$ can be assumed. Thus, letting $\epsilon_{ij} \triangleq \frac{\rho_i}{\sigma_j^2}$ for $i \neq j$ and $\epsilon_{jj} \triangleq \frac{\eta_j}{\sigma_j^2}$, (3) can be rewritten as

$$\mathcal{R} = \log_2\left(1 + \frac{\epsilon_{21}|\boldsymbol{w}_1^H\boldsymbol{H}_{21}\boldsymbol{f}_2|^2}{1 + \epsilon_{11}|\boldsymbol{w}_1^H\boldsymbol{H}_{11}\boldsymbol{f}_1|^2}\right) + \log_2\left(1 + \frac{\epsilon_{12}|\boldsymbol{w}_2^H\boldsymbol{H}_{12}\boldsymbol{f}_1|^2}{1 + \epsilon_{22}|\boldsymbol{w}_2^H\boldsymbol{H}_{22}\boldsymbol{f}_2|^2}\right). \quad (4)$$

As in [15], [16], we shall assume that all channel matrices $\boldsymbol{H}_{ij}$ are known. The beamforming design problem in this FD network can be stated as the maximization of $\mathcal{R}$ in (4) with respect to $\boldsymbol{f}_1$, $\boldsymbol{f}_2$, $\boldsymbol{w}_1$, $\boldsymbol{w}_2$ subject to the following constraints:

1) **Unit-norm constraints:** All four vectors $\boldsymbol{f}_1$, $\boldsymbol{f}_2$, $\boldsymbol{w}_1$, $\boldsymbol{w}_2$ have unit norm.
2) **Constant-amplitude (CA) constraints:** Each of the entries of vectors $\boldsymbol{f}_1$, $\boldsymbol{f}_2$, $\boldsymbol{w}_1$, $\boldsymbol{w}_2$ has constant magnitude.

An upper bound to (4) is obtained assuming no SI ($\epsilon_{11} = \epsilon_{22} = 0$) and dropping the CA constraints. Then $\mathcal{R} \leq \mathcal{R}^\star$, with

$$\mathcal{R}^\star \triangleq \log_2\big(1 + \epsilon_{21}\sigma_1^2(\boldsymbol{H}_{21})\big) + \log_2\big(1 + \epsilon_{12}\sigma_1^2(\boldsymbol{H}_{12})\big) \quad (5)$$

where $\sigma_1(\boldsymbol{A})$ denotes the largest singular value of matrix $\boldsymbol{A}$. Although this upper bound is not achievable in general, it provides a useful benchmark, to be used in Sec. V.

III. The ZF-Max-Power design

Even without CA constraints, maximizing (4) is not a convex problem. An alternative approach suggested in [15] neglects CA constraints and imposes new "Zero-Forcing" (ZF) constraints on the SI. The resulting problem is:

$$P1: \max_{\{\boldsymbol{f}_i\},\{\boldsymbol{w}_j\}} \log_2\left(1 + \epsilon_{21}|\boldsymbol{w}_1^H\boldsymbol{H}_{21}\boldsymbol{f}_2|^2\right) + \log_2\left(1 + \epsilon_{12}|\boldsymbol{w}_2^H\boldsymbol{H}_{12}\boldsymbol{f}_1|^2\right) \quad (6)$$

$$\text{s. to} \quad \|\boldsymbol{f}_1\| = \|\boldsymbol{f}_2\| = \|\boldsymbol{w}_1\| = \|\boldsymbol{w}_2\| = 1, \quad (7)$$

$$\boldsymbol{w}_1^H\boldsymbol{H}_{11}\boldsymbol{f}_1 = \boldsymbol{w}_2^H\boldsymbol{H}_{22}\boldsymbol{f}_2 = 0. \quad (8)$$

We now review this approach in detail as it is the basis of our proposed analog design. Note that the ZF constraints (8) actually cancel SI in the *analog domain,* specifically at the input of the receive RF chains in Fig. 1. However, because of

the coupling between variables due to (8), $P1$ does not admit a closed-form solution. A cyclic maximization-based scheme termed ZF-Max-Power was proposed in [15], which attempts to solve $P1$ iteratively:

1) In the first step, hold the TX beamforming vectors $\boldsymbol{f}_1$, $\boldsymbol{f}_2$ fixed to their values from the previous iteration, and then maximize (6) w.r.t. the RX beamforming vectors $\boldsymbol{w}_1$, $\boldsymbol{w}_2$ subject to the unit norm constraints (7) and the ZF constraints (8). Then the maximization w.r.t. $\boldsymbol{w}_1$, $\boldsymbol{w}_2$ decouples into the following two subproblems:

$$\max_{\boldsymbol{w}_1} |\boldsymbol{w}_1^H \boldsymbol{H}_{21} \boldsymbol{f}_2|^2 \quad \text{s.to} \quad \|\boldsymbol{w}_1\| = 1,\ \boldsymbol{w}_1^H \boldsymbol{H}_{11} \boldsymbol{f}_1 = 0, \quad (9)$$

$$\max_{\boldsymbol{w}_2} |\boldsymbol{w}_2^H \boldsymbol{H}_{12} \boldsymbol{f}_1|^2 \quad \text{s.to} \quad \|\boldsymbol{w}_2\| = 1,\ \boldsymbol{w}_2^H \boldsymbol{H}_{22} \boldsymbol{f}_2 = 0. \quad (10)$$

2) The RX beamforming vectors $\boldsymbol{w}_1$, $\boldsymbol{w}_2$ so obtained are held fixed, and then the maximization is performed w.r.t. $\boldsymbol{f}_1$, $\boldsymbol{f}_2$:

$$\max_{\boldsymbol{f}_1} |\boldsymbol{f}_1^H \boldsymbol{H}_{12}^H \boldsymbol{w}_2|^2 \quad \text{s.to} \quad \|\boldsymbol{f}_1\| = 1,\ \boldsymbol{f}_1^H \boldsymbol{H}_{11}^H \boldsymbol{w}_1 = 0, \quad (11)$$

$$\max_{\boldsymbol{f}_2} |\boldsymbol{f}_2^H \boldsymbol{H}_{21}^H \boldsymbol{w}_1|^2 \quad \text{s.to} \quad \|\boldsymbol{f}_2\| = 1,\ \boldsymbol{f}_2^H \boldsymbol{H}_{22}^H \boldsymbol{w}_2 = 0. \quad (12)$$

These two steps are then iterated until convergence. Some pertinent comments regarding ZF-Max-Power are:

- Each of the corresponding subproblems (9)-(12) can be solved in closed form, as discussed in Sec. IV.
- As in any cyclic maximization procedure, at each step the objective function is increased (or at least not decreased). Since the objective is bounded above, the sequence of values of the objective through the iterations is convergent. This does not necessarily imply convergence to the global maximum of $P1$, although in practice this method seems to work very well [15], [16]: the corresponding solution is often very close to the upper bound (5).
- In order to enforce the original CA constraints, which were neglected in $P1$, the authors of [16] proposed the following. After convergence of ZF-Max-Power, the corresponding solutions for the beamforming vectors are projected onto the set of unit-norm CA vectors

$$\mathcal{V}^N = \left\{ \boldsymbol{v} \in \mathbb{C}^N \,\middle|\, v_i = \frac{1}{\sqrt{N}} e^{j\theta_i},\ i = 1, \ldots, N \right\} \quad (13)$$

  by dividing each entry of the corresponding vector by its magnitude and then scaling the result by the inverse of the square root of the vector dimension. However, this projection step incurs a very significant loss in sum rate.

Thus, although the ZF-Max-Power method seems suitable for digital beamforming systems, it does not provide a satisfactory solution for *analog* beamforming architectures. A modified design overcoming this drawback is presented next.

IV. Proposed analog design

ZF-Max-Power performs poorly with analog beamforming because once the obtained solutions are projected onto the set of CA vectors, the resulting vectors are likely to violate the ZF constraints. The resulting SI may be significant, translating into a large performance loss; this suggests that ensuring that the ZF constraint holds for the final precoders and combiners is of paramount importance. Thus, rather than projecting the final solution after convergence, we propose to seek a vector simultaneously satisfying the ZF and CA constraints *at each iteration* of the cyclic maximization procedure.

Specifically, recall that at each iteration of ZF-Max-Power, subproblems (9)-(12) must be solved. These four subproblems share the same generic form:

$$\max_{\boldsymbol{x}} |\boldsymbol{x}^H \boldsymbol{a}|^2 \qquad \text{s. to} \quad \boldsymbol{x}^H \boldsymbol{c} = 0, \quad \boldsymbol{x}^H \boldsymbol{x} = 1, \qquad (14)$$

where $\boldsymbol{a}, \boldsymbol{c} \in \mathbb{C}^N$ are given vectors and, depending on the particular iteration, $\boldsymbol{x} \in \mathbb{C}^N$ represents either a precoder $\boldsymbol{f}_i$ or a combiner $\boldsymbol{w}_j$. The solution $\boldsymbol{x}_\star$ to (14) is as follows:

$$\widetilde{\boldsymbol{x}} = \left(\boldsymbol{I} - \frac{\boldsymbol{c}\boldsymbol{c}^H}{\|\boldsymbol{c}\|^2} \right) \boldsymbol{a}, \qquad \boldsymbol{x}_\star = \frac{\widetilde{\boldsymbol{x}}}{\|\widetilde{\boldsymbol{x}}\|}, \qquad (15)$$

which can be interpreted as (i) project vector $\boldsymbol{a}$ onto the subspace orthogonal to $\boldsymbol{c}$ to obtain $\widetilde{\boldsymbol{x}}$ (since $\boldsymbol{I} - \frac{\boldsymbol{c}\boldsymbol{c}^H}{\|\boldsymbol{c}\|^2}$ is the projection matrix onto such subspace); (ii) project the result $\widetilde{\boldsymbol{x}}$ onto the set of unit-norm vectors.

In the proposed modification of ZF-Max-Power, we introduce additional constraints in the basic subproblem, so that its solution is a CA vector. Specifically, we replace (14) with

$$\max_{\boldsymbol{x}} |\boldsymbol{x}^H \boldsymbol{a}|^2 \qquad \text{s. to} \quad \boldsymbol{x}^H \boldsymbol{c} = 0, \quad \boldsymbol{x} \in \mathcal{V}^N. \qquad (16)$$

Note that the constraint $\boldsymbol{x} \in \mathcal{V}^N$ subsumes both the CA and unit-norm constraints.

With this additional CA constraint, however, the new subproblem (16) does not have a closed-form solution anymore. Regarding feasibility, a necessary and sufficient condition can be found (see the Appendix for the proof) for the existence of a CA vector orthogonal to a given vector:

Lemma 1. *Let* $\boldsymbol{c} = [\ c_1 \ \cdots \ c_N\ ]^T$. *Then a CA vector* $\boldsymbol{x} \in \mathcal{V}^N$ *satisfying* $\boldsymbol{x}^H \boldsymbol{c} = 0$ *exists if and only if*

$$\frac{1}{N} \sum_{i=1}^{N} |c_i| \geq \frac{2}{N} \max_{1 \leq i \leq N} \{|c_i|\}. \qquad (17)$$

Thus, suppose that the entries of $\boldsymbol{c}$ are random and i.i.d. Under mild assumptions on their distribution, (17) will be satisfied as $N \to \infty$ with probability one. Since N stands for $N_{t,i}$ or $N_{r,j}$ depending on the subproblem, this suggests that feasibility should not be an issue with sufficiently large arrays. In view of this, we propose to tackle (16) by using alternating projections to find a feasible vector. The method of alternating projections is a well-known scheme to seek a point in the intersection of two sets; when the sets are closed and convex, the scheme is known as *projection onto convex sets* (POCS), and it converges to a point in the intersection [17]. In the general case convergence is not guaranteed, but nevertheless the method is routinely applied to nonconvex problems with good results [18].

The proposed iteration to approximately solve (16) is initialized at a point providing a large value of the objective, with the hope that successive projections will remain in its vicinity. Specifically, we set $\boldsymbol{x}^{(0)} = \boldsymbol{a}$, and for $k = 1, 2, \ldots$, do:

1) Projection onto the subspace orthogonal to $\boldsymbol{c}$:

$$\widetilde{\boldsymbol{x}} = \left(\boldsymbol{I} - \frac{\boldsymbol{c}\boldsymbol{c}^H}{\|\boldsymbol{c}\|^2} \right) \boldsymbol{x}^{(k-1)}. \tag{18}$$

2) Projection onto the set of unit-norm CA vectors $\mathcal{V}^N$:

$$x_i^{(k)} = \frac{1}{\sqrt{N}} \frac{\widetilde{x}_i}{|\widetilde{x}_i|}, \qquad i = 1, \ldots, N. \tag{19}$$

These *inner* iterations (alternating projections) should be run for each of the four basic subproblems, which in turn are part of the original, *outer* iterations (cyclic maximization) of ZF-Max-Power. The overall procedure is summarized in Algorithm 1.

Algorithm 1 Precoder-combiner design under CA constraints

function ALTPR($\boldsymbol{a}$, $\boldsymbol{c}$, N)
  $\boldsymbol{x} \leftarrow \boldsymbol{a}$
  for $k \leftarrow 1, N_{\text{inner}}$ **do**
    $\widetilde{\boldsymbol{x}} \leftarrow \boldsymbol{x} - \frac{\boldsymbol{c}^H \boldsymbol{x}}{\|\boldsymbol{c}\|^2} \boldsymbol{c}$
    for $i \leftarrow 1, N$ **do**
      $x_i \leftarrow \frac{1}{\sqrt{N}} \frac{\widetilde{x}_i}{|\widetilde{x}_i|}$
    end for
  end for
  return $\boldsymbol{x}$
end function

Input: $\boldsymbol{H}_{12}$, $\boldsymbol{H}_{21}$, $\boldsymbol{H}_{11}$, $\boldsymbol{H}_{22}$
Initialize $\boldsymbol{w}_1$, $\boldsymbol{f}_1$, $\boldsymbol{w}_2$, $\boldsymbol{f}_2$
for $t \leftarrow 1, N_{\text{outer}}$ **do**
  $\boldsymbol{w}_1 \leftarrow$ ALTPR($\boldsymbol{H}_{21}\boldsymbol{f}_2, \boldsymbol{H}_{11}\boldsymbol{f}_1, N_{r,1}$)
  $\boldsymbol{w}_2 \leftarrow$ ALTPR($\boldsymbol{H}_{12}\boldsymbol{f}_1, \boldsymbol{H}_{22}\boldsymbol{f}_2, N_{r,2}$)
  $\boldsymbol{f}_1 \leftarrow$ ALTPR($\boldsymbol{H}_{12}^H\boldsymbol{w}_2, \boldsymbol{H}_{11}^H\boldsymbol{w}_1, N_{t,1}$)
  $\boldsymbol{f}_2 \leftarrow$ ALTPR($\boldsymbol{H}_{21}^H\boldsymbol{w}_1, \boldsymbol{H}_{22}^H\boldsymbol{w}_2, N_{t,2}$)
end for

V. Numerical results

Consider the setting of Fig. 1 with the two FD nodes having their antennas arranged in uniform linear arrays (ULAs) with $\lambda/2$ separation between adjacent elements (λ is the wavelength). The distance and angle between the TX and RX ULAs of each node are respectively $d = 2\lambda$ and $\omega = \frac{\pi}{6}$ in both cases, see [16, Fig. 2].

For the node-to-node channels $\boldsymbol{H}_{12}$, $\boldsymbol{H}_{21}$, we consider the narrowband clustered channel model from [14], with N_{cl} scattering clusters, each of which contributing N_{ray} propagation paths. The channel matrices are then given by

$$\boldsymbol{H}_{ij} = \sum_{k=1}^{N_{\text{cl}}} \sum_{\ell=1}^{N_{\text{ray}}} \beta_{k,\ell} \boldsymbol{a}_{\text{r}}(\phi_{k,\ell}^j) \boldsymbol{a}_{\text{t}}^*(\theta_{k,\ell}^i), \tag{20}$$

with $\beta_{k,\ell}$ the complex gain of the ℓ^{th} ray in the k^{th} cluster, and $\boldsymbol{a}_{\text{t}}(\theta_{k,\ell}^i)$ and $\boldsymbol{a}_{\text{r}}(\phi_{k,\ell}^j)$ the antenna array steering and response vectors at the transmitter and receiver, respectively, evaluated at the corresponding azimuth angles of departure from transmitter at node i, $\theta_{k,\ell}^i$, or arrival at node j, $\phi_{k,\ell}^j$. In the simulations, we take $N_{\text{cl}} = 6$ clusters and $N_{\text{ray}} = 8$ paths per cluster. The path gains are independently drawn from a circular complex Gaussian distribution, all with the same variance. The angles of departure and arrival are random, with uniformly distributed mean cluster angle and angular spreads of 20°.

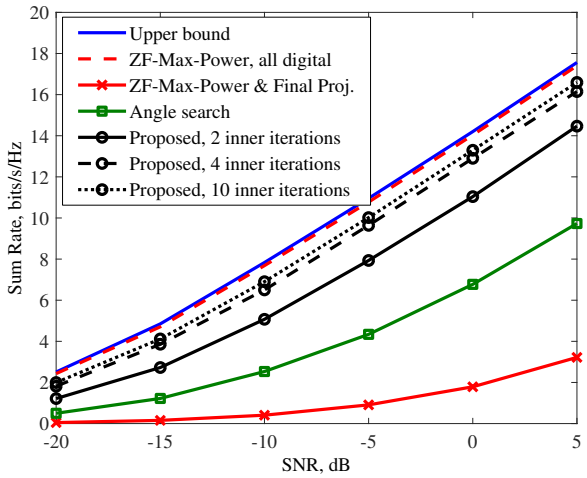

Fig. 2. Performance results (500 Monte Carlo runs). Self-interference to noise ratio is 30 dB at both nodes. $N_{t,1} = N_{t,2} = 32$, $N_{r,1} = N_{r,2} = 16$.

We assume that the TX and RX arrays of each node are close to each other, so that a line-of-sight near-field model is adopted for the SI channels $\boldsymbol{H}_{11}$, $\boldsymbol{H}_{22}$ [3], [4], [15], [16]:

$$[\boldsymbol{H}_{ii}]_{pq} = \frac{1}{d_{pq}^{(i)}} e^{-j2\pi \frac{d_{pq}^{(i)}}{\lambda}}, \tag{21}$$

with $d_{pq}^{(i)}$ the distance between the p-th antenna of the TX array and the q-th antenna of the RX array of node i. All channel matrices are normalized so that $\text{tr}\, \boldsymbol{H}_{ij}^H \boldsymbol{H}_{ij} = N_{t,i} N_{r,j}$.

Fig. 2 shows the sum rate obtained by different designs, in terms of the SNR $\epsilon_{12} = \epsilon_{21}$ which is set equal at both nodes, when the array sizes are $N_{t,1} = N_{t,2} = 32$ and $N_{r,1} = N_{r,2} = 16$. The SI-to-noise ratios are $\epsilon_{11} = \epsilon_{22} = 30$ dB. For ZF-Max-Power, 50 cyclic-maximization iterations were run. In the proposed design, for each of those 50 outer iterations, different number of alternating-projection inner iterations were tested. In all cases, the precoders and combiners were randomly initialized.

The performance of the all-digital (i.e., no CA constraint) ZF-Max-Power design is very close to the upper bound (5), but when the corresponding solution is projected onto the set of CA vectors (method 2 from [16]), a very significant performance loss is observed, in agreement with [16]. The angle search approach (method 1 from [16]) performs somewhat better at the price of a much higher computational cost. In contrast, the proposed design is able to provide a CA solution at a moderate loss with respect to the all-digital solution (within 1.2 dB with 10 inner iterations). A feasible solution was found in all Monte Carlo trials.

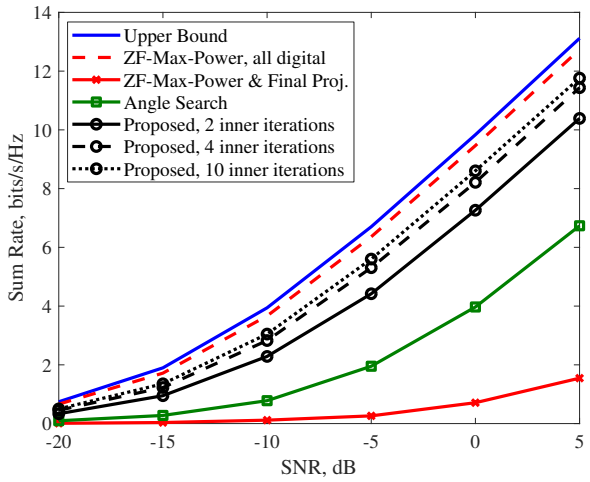

Fig. 3. Performance results (500 Monte Carlo runs). Self-interference to noise ratio is 30 dB at both nodes. $N_{t,1} = N_{t,2} = 8$, $N_{r,1} = N_{r,2} = 8$.

Fig. 3 shows results under the same conditions, except for the array sizes which were set to $N_{t,1} = N_{t,2} = 8$ and $N_{r,1} = N_{r,2} = 8$; similar trends to those in Fig. 2 can be observed. Again, a feasible solution was always found, even for these relatively small array sizes. In this case, with 10 inner iterations the proposed method approaches the all-digital design within 1.4 dB.

VI. Conclusion

We have proposed an effective design of analog beamformers for Full-Duplex mmWave communication, simultaneously achieving spatial SI suppression and sizeable beamforming gain. This design is based on the method of alternating projections and exhibits convergence in a few iterations, without any noticeable feasibility problems. As with any beamforming design, knowledge of the channel matrices involved is required. In particular, estimation of mmWave SI channels is not a well-studied area, clearly deserving future attention.

Appendix: Proof of Lemma 1

Without loss of generality, assume that $|c_1| \geq |c_2| \geq \cdots \geq |c_N|$. Note that the existence of a CA vector $\boldsymbol{x} \in \mathcal{V}^N$ with $\boldsymbol{x}^H \boldsymbol{c} = 0$ is equivalent to the existence of a polygon in $\mathbb{R}^2$ with sides $|c_1|$, $|c_2|$,...,$|c_N|$.

Suppose first that (17) does not hold, i.e., $|c_1| > |c_2| + \cdots + |c_N|$. Since for any a, $b \in \mathbb{C}$ it holds that $|a+b| \geq |(|a|-|b|)|$, one has that, for any angles θ_1,...,θ_N,

$$\begin{aligned} \left| \sum_{i=1}^{N} c_i e^{j\theta_i} \right| &\geq \left| \left(|c_1| - \left| \sum_{i=2}^{N} c_i e^{j\theta_i} \right| \right) \right| \\ &\geq \left| \left(|c_1| - \sum_{i=2}^{N} |c_i| \right) \right| > 0, \end{aligned} \tag{22}$$

which proves the first part of the result.

To prove the second part, assume now that (17) does hold, i.e., $|c_1| \leq |c_2| + \cdots + |c_N|$, and let us find a valid polygon. If $N = 2$, the proposition is trivial because then $|c_1| = |c_2|$. If $N = 3$, the result follows from the fact that a triangle (degenerate if $|c_1| = |c_2| + |c_3|$) with sides $|c_1|$, $|c_2|$ and $|c_3|$ can be constructed. If $N > 3$, we proceed iteratively as follows. Let $\mathcal{L}_0 = \{\ell_i^{(0)}, 1 \leq i \leq N\}$ with $\ell_i^{(0)} \triangleq |c_i|$, $1 \leq i \leq N$. For $k \geq 1$, let $\mathcal{L}_k = \{\ell_i^{(k)}, 1 \leq i \leq N-k\}$ be the set obtained from $\mathcal{L}_{k-1}$ by adding its two smallest elements and keeping the rest, and then reordering so that $\ell_1^{(k)} \geq \ell_2^{(k)} \geq \cdots \geq \ell_{N-k}^{(k)}$. Clearly, at each stage the inequality $\ell_1^{(k)} \leq \ell_2^{(k)} + \cdots + \ell_{N-k}^{(k)}$ holds. Therefore, for $k = N-3$ it is possible to construct a triangle with sides $\ell_1^{(N-3)}$, $\ell_2^{(N-3)}$ and $\ell_3^{(N-3)}$, which is the desired polygon.

References

[1] R. W. Heath Jr., N. González-Prelcic, S. Rangan, W. Roh and A. Sayeed, "An overview of signal processing techniques for millimeter wave MIMO systems," *IEEE J. Sel. Topics Signal Process.,* vol. 10, no. 3, pp. 436–453, Apr. 2016.

[2] 3GPP "Physical channels and modulation. Release 15," TS 38.211, https://portal.3gpp.org/desktopmodules/Specifications/SpecificationDetails.aspx?specificationId=3213, Mar. 2018.

[3] Liangbin Li, K. Josiam and R. Taori, "Feasibility study of full-duplex wireless millimeter-wave systems," *Proc. IEEE Int. Conf. Acoust., Speech, Signal Process.,* 2014, pp. 2769–2773.

[4] S. Rajagopal, R. Taori and S. Abu-Surra, "Self-interference mitigation for in-band mmWave wireless backhaul," *Proc. IEEE Consumer Commun. Netw. Conf.,* 2014, pp. 551–556.

[5] A. Sabharwal, P. Schniter, D. Guo, D. Bliss, S. Rangarajan and R. Wichman, "In-band full-duplex wireless: Challenges and opportunities," *IEEE J. Sel. Areas Commun.,* vol. 32, no. 9, pp. 1637–1652, Sep. 2014.

[6] Z. Zhang, K. Long, A. V. Vasilakos and L. Hanzo, "Full-duplex wireless communications: Challenges, solutions, and future research directions," *Proc. IEEE,* vol. 104, no. 7, pp. 1369–1409, Jul. 2016.

[7] D. Bharadia, E. McMilin, and S. Katti, "Full duplex radios," in *Proc. ACM SIGCOMM,* Hong Kong, China, Aug. 2013, pp. 375–386.

[8] M. Heino, D. Korpi, T. Huusari, E. Antonio-Rodriguez, S. Venkatasubramanian, T. Riihonen, L. Anttila, K. Haneda, R. Wichman and M. Valkama, "Recent advances in antenna design and interference cancellation algorithms for in-band full-duplex relays," *IEEE Commun. Mag.,* vol. 53, no. 5, pp. 91–101, May 2015.

[9] F. Sohrabi and W. Yu, "Hybrid digital and analog beamforming design for large-scale MIMO systems," *Proc. IEEE Int. Conf. Acoust., Speech, Signal Process.,* 2015, pp. 2929–2933.

[10] E. Zhang and C. Huang, "On achieving optimal rate of digital precoder by RF-baseband codesign for MIMO systems," *Proc. IEEE Veh. Technol. Conf.,* Sep. 2014, pp. 1–5.

[11] B. Day, A. Margetts, D. Bliss and P. Schniter, "Full-duplex bidirectional MIMO: Achievable rates under limited dynamic range," *IEEE Trans. Signal Process.,* vol. 60, no. 7, pp. 3702–3713, Jul. 2012.

[12] S. Huberman and T. Le-Ngoc, "MIMO full-duplex precoding: A joint beamforming and self-interference cancellation structure," *IEEE Trans. Wireless Commun.,* vol. 14, no. 4, pp. 2205–2217, Apr. 2015.

[13] E. Everett, C. Shepard, L. Zhong, and A. Sabharwal, "SoftNull: Many-antenna full-duplex wireless via digital beamforming," *IEEE Trans. Wireless Commun.,* vol. 12, no. 15, pp. 8077–8092, Dec. 2016.

[14] O. El Ayach, S. Rajagopal, S. Abu-Surra, Z. Pi, R. W. Heath, Jr., "Spatially sparse precoding in mmWave MIMO systems," *IEEE Trans. Wireless Commun.,* vol. 13, no. 3, pp. 1499–1513, Mar. 2014.

[15] Xiao Liu, Zhenyu Xiao, Lin Bai, Jinho Choi, Pengfei Xia and Xiang-Gen Xia, "Beamforming based Full-Duplex for millimeter-wave communication," *Sensors,* 16, 1130, Jul. 2016.

[16] Zhenyu Xiao, Pengfei Xia and Xiang-Gen Xia, "Full-Duplex millimeter-wave communication," *IEEE Wireless Commun.,* pp. 136–143, Dec. 2017.

[17] L. M. Bregman, "The method of successive projection for finding a common point of convex sets," *Soviet Mathematics,* 6, pp. 688–692, 1965.

[18] R. Escalante and M. Raydan, *Alternating projection methods.* Society for Industrial and Applied Mathematics, vol. 8, 2011.